Monitoring and Diagnosing the Natural Deterioration of Multi-Stage Helical Gearboxes based on Modulation Signal Bispectrum Analysis of Vibrations

James Xi Gu[1], Alhussein Albarbar[3], Xiuquan Sun[2,*], Anwar M Ahmaida[2], Fengshou Gu[2], and Andrew. D. Ball[2]

[1] School of Engineering, University of Bolton, Bolton BL3 5AB, UK
[2] Centre for Efficiency and Performance Engineering, University of Huddersfield, Huddersfield, HD1 3DH, UK
[3] Department of Engineering, Manchester Metropolitan University, Manchester, M15 6BH

Abstract

Understanding development stages of gear failures e.g. progressive tooth wear, fatigue pitting and micro cracks is the key for effective gearbox condition monitoring systems. This paper presents a novel method for diagnosing gradual deterioration of gears using Modulation Signal Bispectrum (MSB) and vibration measurements. A nonlinear model was derived to understand dynamic forces applied to gears that are excited by quadratic terms e.g. shaft rotating speeds and gear meshing frequencies. Owing to its sensitivity to those quadratic terms, MSB is powerful in recovering less noisy condition related features from the measured vibration signals e.g. gear meshing and multiples of shaft rotating speed. This allows more pronounced representation of gears dynamic forces and makes it more effective for detecting early gear deterioration. The proposed method was verified through a run-to-failure test based on a multiple-stage helical gearbox transmission system. Results show small gears at low speed stages deteriorate faster and fail at 838 hours. This was because they prone to wear more sever due to poorer lubrication conditions compared with gears at high speed stages. Moreover, fault detectability of the developed MSB based method outperforms that of Time Synchronous Averaging (TSA). Compared to TSA, clearer signs of early gear deterioration was captured using MSB, which makes it more powerful tool for monitoring the condition of gearboxes.

Keywords: Vibration Condition Monitoring, Gearbox Deterioration, Modulation Signal Bispectrum, Time Synchronous Averaging (TSA), Gear Condition Indicator (GCI), Remaining Useful Life (RUL).

1 Introduction

Gradual gear deterioration including on-going tooth wear, fatigue pitting and cracks is an inevitable phenomenon in the lifetime of operational gears. In general, gear wear process is considered as progressive material loss at the mating surfaces resulted from both rolling motion and sliding motion effects under poor lubrication conditions [1][2]. Severe wear can lead to uneven load distribution that, if persists, may lead to other faults including pitting, scoring and even tooth breakage. For these reasons, monitoring gear wear has attracted attention of condition monitoring community in an effort to ensure safe operation and to avoid unexpected catastrophic failures in rotating machines.

Many methods have been proposed for detecting wear in gears e.g. wear particle analysis [3] has been popularly used for monitoring the gear wear severity. Normally, the accumulated wear is taken as a key parameter for monitoring total wear. Moreover, motion inconsistency between any surfaces in contact forms debris which can be used to detect and determining wear severity [4][5]. At present, most wear particle analysis are carried out off-line using expensive instruments. While some methods have been

developed for on-line lubrication monitoring, the accuracy is inconsistent due to differences in oil sampling procedures. Moreover, those methods are time-consuming and expensive to carry out.

Gear vibration signals are rich of dynamic features that are suitable for real-time condition monitoring of various faults in rotating machinery. Vibration analysis has been in use for decades for detecting localised gear faults such as tooth cracks. However for progressive tooth wear and micro-pitting, the relative studies are still limited. This is mainly due to low signal-to-noise ratio (SNR) from such incipient faults, which creates high challenges to develop data processing methods [4]. Nevertheless, in recent years, several vibration-based studies were carried out experimentally and numerically to monitor the gear wear conditions. Hu et al. [6] extracted gear state vector from the time synchronous averaged signal, then calculated two averaged logarithmic ratios to reflect the wear degree based on the sidebands information contained. An integrated approach of using wear debris and vibration analysis was put forward by Peng [7] to diagnose machinery faults like pitting and wear. Jozef [8] investigated the influence of the deformation and wear on the gear dynamics experimentally and analytically. Ding [9] introduced a dynamic model combined with wear model for predicting the nonlinear effects induced by gear backlash and time-varying mesh stiffness. The results show that the wear has significant influences on the amplitude of each harmonic component of the response in different levels. To accurately extract the weak signature at early stages of gear deteriorations, many signal processing techniques have been proposed and improved for vibration analysis. Among those techniques, time synchronous averaging (TSA) [10][11][12] is considered to be one of the most effective methods because of its unique properties in noise reduction and mesh components enhancement. Based on TSA analysis, a large number of condition indicators (GCIs) have developed for vibration-based gearbox monitoring. Of most interesting ones are NA4, ER, FM4, NB4, kurtosis and so on, showing good performance to indicate gear health conditions[13] [14]. Especially, the higher orders of centralized moments in these GCIs allow the changes in signals due to gear faults to be highlighted sufficiently. However, the accuracy of TSA relies highly on the information of the angular position of gears and the phase error accumulation effect could cause a reduction in the amplitude of the useful features with the increase of averaging times[15] and its implementation is computationally expensive. In addition, it needs additional measurements to get phasor signals, which increase the cost of monitoring system. Moreover, the condition is assessed by statistical parameters, which are not reliable due to poor accuracy and instability.

Recently, limitation of TSA based analysis have been mitigated by the development of Modulation Signal Bispectrum (MSB) based analysis technique. MSB is an excellent technique for detecting and diagnosing incipient faults in rotation machines including reciprocating compressors [16], induction motors [17], rolling bearings [18], centrifugal pumps [19] and so on. It was also used for tracing gradual changes in vibration and motor current signals to indicate gearbox deteriorations [20][21].

Based upon the above surveyed research work, MSB monitoring capabilities have not yet been assessed and benchmarked sufficiently. Via a detailed mathematical model, this study will first investigate effects of gear transmission dynamics on the measured vibrations. This would include difficulties in capturing condition related features from the noisy vibration data and the need for more powerful analysis techniques e.g. MSB. Second, a new scheme is developed to monitor gradual deterioration of gears based on fusion of multiple MSB peak magnitudes. Third, performance of the proposed scheme is evaluated using experimental run-to-failure testing data for multiple stage helical gearbox system. Finally, the obtained results are compared to those obtained using TSA technique alongside critical comments on performance of the developed new scheme.

2 Dynamics of Gear Transmissions

It was demonstrated that MSB analysis is particularly effective in characterising the interconnection of phases and frequencies in modulation signals such as gear vibration responses [17]-[21]. However,

MSB magnitude behaviours have not been addressed sufficiently in association with gear dynamics. This section shows that the dynamic forces consisting of different orders of coupled quadratic terms can be better captured and emphasised using MSB analysis.

2.1 Dynamic Model

As shown in Fig. 1, a helical gear transmission can be commonly modelled to have both translational and rotational motions by following comprehensive governing equations based on the studies such as [22] :

$$\begin{cases} m_g\ddot{y}_g + c_{by}\dot{y}_g + k_{by}y_g = F_{my} + F_{iy} \\ m_g\ddot{z}_g + c_{bz}\dot{z}_g + k_{bz}z_g = -F_{mz} + F_{ix} \\ m_g\ddot{x}_g + c_{bx}\dot{x}_g + k_b x_g = F_f + F_{iz} \\ I_g\ddot{\theta}_g = T_d - F_{my}r_{bg} \\ m_p\ddot{y}_p + c_{by}\dot{y}_p + k_b y_p = -F_{my} + F_{iy} \\ m_p\ddot{z}_p + c_{bz}\dot{z}_p + k_{bz}z_p = F_{mz} + F_{iz} \\ m_p\ddot{x}_p + c_{bx}\dot{x}_p + k_{bx}x_p = F_f + F_{iz} \\ I_p\ddot{\theta}_p = T_L - F_{my}r_{bp} \end{cases} \tag{1}$$

where I_i is the moment of inertia, the subscript i=p, g denotes pinion and gear respectively; m_i denotes the mass of the gear, θ_i represents the angle of rotation; $x, \dot{x}, \ddot{x}$ denotes the translational displacement, velocity and acceleration in x-direction respectively, and the same for y- and z-directions; c_b and k_b respectively denotes the damping constant and stiffness constant of the bearing. T_d, T_L are the loads applied to the driving gear and driven pinion; r_{bg}, r_{bp} are the radius of the base circle of gear and pinion; F_m, and F_f are nonlinear and periodically varying mesh forces due to variation in stiffness and friction in a mesh cycle, respectively, which can be obtained by:

$$F_m = c_m\dot{\delta} + k_m f(\delta) \tag{2}$$

$$F_f = \mu(t)[c_m\dot{\delta} + k_m f(\delta)] \tag{3}$$

where k_m, and c_m are stiffness and damping respectively, $\mu(t)$ is the time-varying friction coefficient, $f(\delta)$ is the dynamic transmission error function in which δ is the relative displacement:

$$\delta = \left(y_g + r_{bg}\theta_g\right) - \left(y_p - r_{bp}\theta_p\right) + e_{pg} \tag{4}$$

where e_{pg} is the comprehensive transmission error. It is worth of noting that these dynamic forces are stemmed from the nonlinear interaction between the periodic stiffness and system response. To show its magnitude behaviour it is necessary to analytically examine the basic characteristics of both terms based on the nonlinear mechanism of a gear transmission.

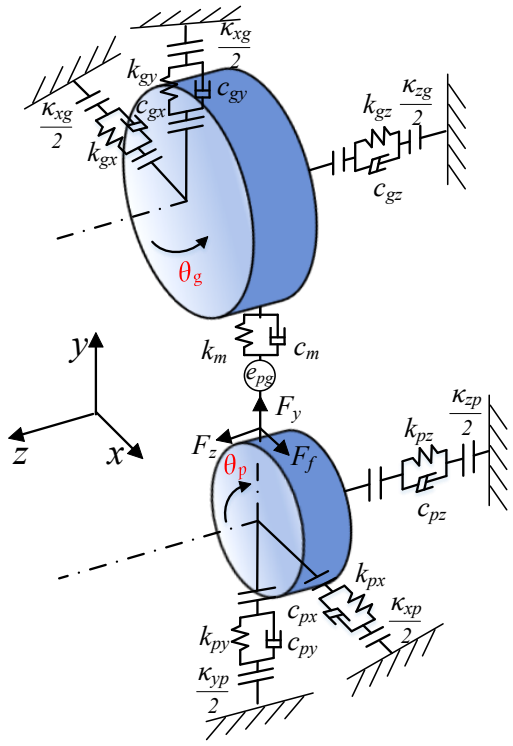

Figure 1 typical dynamic model of a gear pair

2.2 Nonlinear Time-varying Stiffness

As the primary excitation for vibration systems, time-varying stiffness has received considerable investigations for gear condition monitoring purposes [23] [24] [31][32]. In general, considering various tooth deformations $\sum \epsilon_{pg}$ due to load, and errors e_{pg} due to manufacturing imperfection and potential faults such as wear and pitting, the tooth stiffness for a pair of gear can be represented by

$$k = \frac{\mathrm{F}}{\sum \epsilon_{pg} + e_{pg}} \tag{5}$$

As stiffness varies with time periodically at mesh frequency f_m and the error is usually associated with each gear and varies at rotation frequency f_r, the stiffness that takes into account error effects can be approximated by Eq.(6), as a consequence of the nonlinear interaction between f_m and f_r waves in terms of Fourier series

$$k_m(\mathrm{t}) = \bar{k}_m[1 + \sum_j k_{je}(2\pi j f_r t + \theta_{je})] \sum_i \kappa_i \cos(2\pi i f_m \mathrm{t} + \theta_i)] \tag{6}$$

For further analytic studies, Eq. (6) can be expressed more simply with two terms: $A_{f_m} k_m(\mathrm{t})|_{f_m}$ and $A_{f_r} k_r(\mathrm{t})|_{f_r}$ which represent the mesh components and rotation components respectively. This yields

$$k_m(\mathrm{t}) = A_{f_m} k(\mathrm{t})|_{f_m} + A_{f_m} k(\mathrm{t})|_{f_m} A_{f_r} k_r(\mathrm{t})|_{f_r} \tag{7}$$

which avoids the complexity of exploring the multiple terms of Fourier series but highlights just two main terms. In particular, the first term shows the high frequency carrier contents associated with f_m and the second term shows the modulation induced sidebands resulted from the nonlinear coupling between the f_m and f_r waves.

2.3 Modulation Response of Steady Operation

Based on the form of stiffness excitation of Eq. (6), a typical steady solution of a translational response in the principal direction y can be expressed by a generic signal model [25][26] in the same form of modulations as Eq.(6):

$$y(t) = \sum_m C_m[1 + a_r(t)]\cos\left[2\pi m f_m \mathrm{t} + p_r(t) + \theta_m\right] + n(t) \tag{8}$$

which consists of a carrier wave due to gear mesh components f_m:

$$c_m(t) = \sum_m C_m \cos[2\pi m f_m \mathrm{t} + \theta_m];$$

and amplitude modulation (AM) and phase modulation (PM) due to rotation components f_r

$$\text{AM wave: } a_r(t) = \sum_r A_r \cos\left[2\pi r f_r \mathrm{t} + \theta_a\right]$$

$$\text{PM wave: } p_r(t) = \sum_r P_r \cos\left[2\pi m f_r \mathrm{t} + \theta_p\right]$$

Both types of modulations are due to the effect of gear errors including erroneous tooth profiles due to not only manufacturing but also progressive wear, pitting and cracks although PM is often more related to speed variations. This basic model has been widely accepted in the condition monitoring community for developing more effective data analytic techniques [27].

Moreover, $n(t)$ in Eq.(8) denotes the inevitable Gaussian noise to take into account noise influences from measurement systems and any randomness due to uncertain factors such as ambient changes and so on. Suppressing $n(t)$ is very critical for obtaining a reliable deterministic feature parameter for gear condition monitoring in terms of not only enhancing the weak features for detecting incipient faults but also stabilising condition indicators for diagnostics and prognostics.

For the small rotation variations during quasi-steady operations, PM effect is less significant. The phase modulation nonlinearity in Eq.(8) can be simplified via a linearisation scheme such as [29]. This can result in a simplified expression for general responses, which consist of nonlinear couplings between three waves: $C_{f_m} c(t)|_{f_m}$ from mesh effect, $A_{f_r} a(\mathrm{t})|_{f_r}$ from AM and $P_{f_r} p\big(t - \pi - \theta_{ap}\big)|_{f_r}$ from PM for the mesh and rotation responses are shown in Eq. (9).

$$y(t) = C_{f_m} c(t)|_{f_m} + C_{f_m} c(t)|_{f_m} A_{f_r} a(t)|_{f_r} + C_{f_m} c(t)|_{f_m} P_{f_r} p\big(t - \pi - \theta_{ap}\big)|_{f_r} \tag{9}$$

It is worth pointing out PM waves oscillate at the same frequencies as those of AM. However, there are phase differences θ_{ap} between these two modulating waves due to difference in underlying physics. In fact, it is this phase difference that the asymmetric amplitudes are often observed between lower and higher sidebands around mesh frequency. However, influences of PM are negligible as they are much smaller due to high moments of inertia.

2.4 Characteristics of Dynamic Forces

For more understandings of dynamic forces, the interaction between stiffness and vibration responses are examined by considering effects of only displacement influences shown in Eq.(2). The interaction between velocity response and damping effect can have the same form as that of displacement. For ease of analysis, the effects of velocity are not examined in this study.

As stiffness expressed in Eq. (6) and response in described in Eq. (8) share the same waveform frequency content and resulted modulation, multiplication between stiffness and displacement response referred to in Eq. (2) can be expressed as the square of Eq. (10).

$$F_m(\mathrm{t}) = [C_{f_m} c(t)|_{f_m} + C_{f_m} c(t)|_{f_m} A_{f_r} a(t)|_{f_r}) + C_{f_m} c(t)|_{f_m} P_{f_r} p\big(t - \pi - \theta_{ap}\big)|_{f_r}]^2 \tag{10}$$

In case of considering AM only i.e. ignoring high orders of small PM effects, Eq.(10) is approximated to Eq. (11).

$$F_m(\mathrm{t}) \approx \left[C_{f_m} c(t)|_{f_m}\right]^2 \left[A_{f_r} a(t)|_{f_r}\right]^2 + [C_{f_m} c(t)|_{f_m}]^2 + 2[C_{f_m} c(t)|_{f_m}]^2 A_{f_r} a(t)|_{f_r} \tag{11}$$

Clearly, the amplitude of dynamic forces can be characterised by multiple coupled quadratic terms (CQT) and nonlinear combination of the two primary waves at various meshing components f_m and rotation components f_r. Therefore, these quadratic terms and their nonlinear combination in the responses should be highlighted in order to truly reflect the effect of dynamic forces on gear condition. Hence, this novel finding paves the foundation for the use of higher order spectra including MSB analysis. In particular, this is significantly different from conventional analysis that focus on separation of different waves and linear combination afterwards.

3 Application of MSB Analysis Technique

3.1 Noise Suppression

Due to inevitable noise in the measured vibration signals, many methods have been developed and investigated to extract such nonlinear effects. TSA is one of the most effective methods in which time-based vibration signals are synchronised. This is to identify and filter out random phases noise components or those are not synchronised with any shaft speed. By applying order analysis on the synchronised signals, various sidebands and mesh components are separated for further feature extraction. The main deficiency is that TSA needs an additional phasor signal from an external encoder. This increases the cost of the condition monitoring system and makes it not suitable for multiple stage gear transmissions as more encoders are required. There are also other disadvantages associated with TSA e.g. less accurate, less efficient as it needs high order of interpolation sample by sample.

Recently MSB analysis has been applied to vibration, acoustics and instantaneous current signals collected from electromechanical machines [17][18][19]. MSB has been found highly effective in extracting incipient fault signatures from the monitored data. The MSB originated from the conventional bispectrum by additionally considering the lower sideband to describe modulation signals more accurate. Eq. (12) expressed MSB in the frequency domain.

$$B_{MS}(f_r, f_m) = E\langle Y(f_m + f_r)Y(f_m - f_r)Y^*(f_m)Y^*(f_m)\rangle \tag{12}$$

where, f_c and f_x denote the coupled frequency components. $E\langle\ \ \rangle$ is the ensemble average of MSB matrix obtained from the multiple segments of the modulation signals. $Y(f) = \int_{-\infty}^{+\infty} y(t)e^{-i2\pi ft}\,dt$ is the Fourier transform of the signal $y(t)$.

For an AM/PM signal when only individual modulation is considered in the gear vibration response of Eq. (6), the phase of the MSB can be calculated from:

$$\phi(f_r, f_m) = \phi(f_m + f_r) + \phi(f_m - f_r) - \phi(f_m) - \phi(f_m) \tag{13}$$

When the components f_c and f_x are coupled by amplitude modulation (AM) or phase modulation (PM), the subsequent phase has the relationship as

$$\begin{aligned} \phi(f_m + f_r) &= \phi(f_m) + \phi(f_r) \\ \phi(f_m - f_r) &= \phi(f_m) - \phi(f_r) \end{aligned} \tag{14}$$

Consequently, the resultant phase of the MSB phase $Y(f_c + f_r)Y(f_c - f_r)Y^*(f_c)Y^*(f_c)$ will be zero for pure AM signals or $\pm\pi$ for PM signals, which are valid for any segments windowed from a long time series.

If the signal is a combination of AM and PM effect, which is the general case of gear dynamics, the phase for each segment is within the range of $[0, \pm\pi]$ and remains the same for the stationary process. So the resulted MSB peak will also have a phase value within $[0, \pm\pi]$.

Based on this phase invariance property of modulation signals, the phases between different signal segments are aligned. By ensemble averaging, the modulation amplitude is enhanced greatly so that its

peaks are stabilised. Simultaneously, the random noises and non-modulation components are suppressed because their phases are random between different signal segments.

Similar to the normalisation way of conventional bicoherence, the coherence of MSB can be defined as

$$b_{MS}(f_r, f_m) = \frac{|B_{MS}(f_r, f_m)|^2}{E\langle|Y(f_m)Y^*(f_m)|^2\rangle E\langle|Y(f_m + f_r)Y(f_m - f_r)|^2\rangle} \quad (15)$$

The MSB coherence allows to indicate the degree of coupling and noise suppression among the modulation components. The MSB coherence is in the range from 0 to 1, which is independent of the amplitude of the coupled components in the frequency domain. If the coherence is close to 0, it means there is no correlation between the components. This means they are either independent components or different random noises. If coherence value is close to 1, this indicates the interaction between the components such as f_r and f_m and their harmonics is strong but still slightly influenced by noise. Based on the property of coherence, the MSB magnitude can be further checked for the reliability of analysis.

3.2 Magnitude Enhancement of Gear Vibration

Initial phases such as θ_m, θ_a and θ_p shown in Eq. (8) can be ignored as they do not contribute into amplitudes. Thus the interaction of the first order of waves in Eq. (8) can be observed at three frequencies: $(f_m - f_r)$, $(f_m + f_r)$, and (f_m) in the form of :

$$y(t) = C_m \cos[2\pi m f_m \mathrm{t} + \theta_m] + A_r C_m/2 \cos[2\pi(f_m - f_r)\mathrm{t}] + A_r C_m/2 \cos[2\pi(f_m + f_r)\mathrm{t}] \quad (16)$$

It shows that the amplitudes at sidebands are multiplication of carrier and modulating waves. According to Eq. (13), the magnitude of MSB will be:

$$|MSB| = A_r^2 C_m^4/4 \quad (17)$$

Due to the products between sidebands and mesh components, MSB magnitudes can be more consistent with the dynamic forces as shown in Eq. (11) that consists of a series of coupled quadratic terms. Therefore, it is more adequate to use MSB to interpret vibration results.

In addition, to exclude the amplitude contribution of mesh waves to MSB magnitude, a MSB sideband estimator (shorten as MSB-SE) can be used, which can be easily obtained by normalising MSB by the carrier amplitude and taking account of phase effect of the carrier in the process of MSB calculation via:

$$MSB_{MS}^{SE}(f_r, f_m) = E\left\langle Y(f_m + f_r)Y(f_m - f_r)e^{-i2\phi(f_m)t}\right\rangle \quad (18)$$

This leads to an interacted magnitude:

$$|MSB - SE| = A_r^2 C_m^2/4 \quad (19)$$

That is a further approximation to represent the magnitude of gear dynamic force in Eq. (12).

In general, not only MSB can suppress random noise in the gear vibration signals but also give a more straight indication of the dynamic forces applying to the vibration system because its magnitudes is a direct fusion between mesh and rotation components. Besides, MSB can be implemented efficiently and conveniently as it can be estimated by FFT algorithm widely available in various software packages. There is no need for external phasor measurements like those required for TSA.

4 Run-to-Failure Experimentation

4.1 Test System

In most cases, gear tooth wear occurs due to the effects of different lubrication regimes and contamination. Under different speeds and loading conditions, wear progresses proportionally to

operating time and this causes different vibration responses. For more realistic and practical verification, run-to-failure tests have been performed on a test rig shown in Figure 2. The rig consists of multi-stage helical gearboxes, similar to those used in wind turbines, vehicle power transmissions and helicopters. The experimental aim is to achieve precise progressive wear in order to investigate different phases of lifespans and consequently predict the progression of gear gradual deteriorations based on vibration analysis.

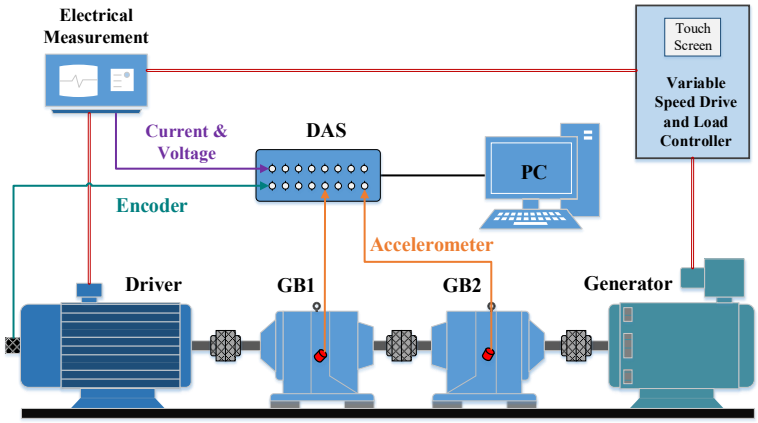

Figure 2 Schematic of helical gearbox test system

The test rig comprises two 10kW helical gearboxes installed back-to-back for tests, detailed in Figure 3 and Table 1. They are connected to a15kW AC drive motor and the DC load generator by flexible links respectively. The operating conditions (load and speed) were controlled by a variable speed drive (VSD) and a load controller. The VSD ensures that the speed of the AC motor is as steady as possible at the set speed and load. Gearbox 1 (GB1) act as a speed reducer and Gearbox 2 (GB2) as a speed increaser. This transmission layout allows sufficient loads applied to the system by the 17 kW DC generator which usually needs to run in high speed ranges, above 1000 rpm. Both gearboxes were from a major gearbox manufacturer, which are used widely in different industries such as airport conveyors, rolling machines, vacuum pumps and so on. The main technical specifications of the two helical gearboxes used in this study are shown in Table 1. The gears at the low speed stages are the same for two gearboxes whereas the high speed stage transmission ratio or gear teeth in GB2 is different from that of GB1. This arrangement allows for efficient and effective tests as it can have the vibration dataset of the natural deteriorations for two sets of same gears and 2 sets of different gears to be investigated for vibration based monitoring.

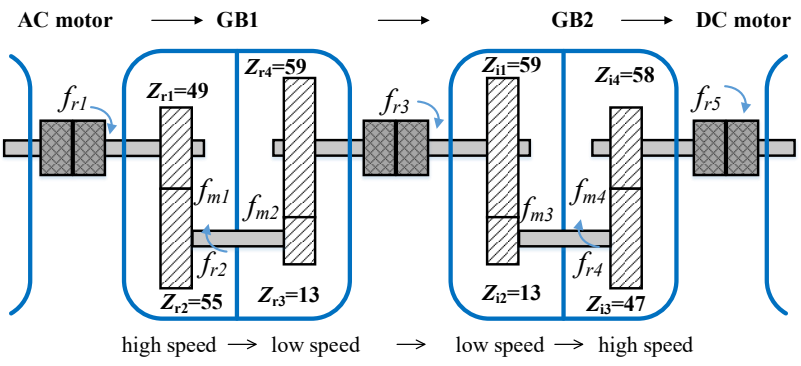

(a) Schematic of two gearboxes

(b) Internal structure of gearbox

Figure 3 System layout of helical gear transmissions (shaft and gear joints)

In order to achieve the on-line monitoring of gear conditions, two vibration accelerometers were mounted on the middle of housing of two gearboxes respectively for collecting vibration signals, shown

in Figure 2. This sensor position allows the dynamics of gears at both speed stages to be perceived with just one sensor, as the sensor is closer to the internal supporting brackets for the gears of two speed stages, as illustrated in Figure 3 (b). The sensors have a sensitivity of 50 mV/g and a linear frequency band up to 10kHz, which have been demonstrated by trial tests to be sufficient to undertake the vibration amplitudes and cover the resonances of the gear systems.

The vibration signals along with shaft encoder signal, instantaneous electric signatures and oil temperature were collected by a 16-channel data acquisition system operating at a 96kHz sampling rate and 24 bit resolution. The high data accuracy to ensure that the small changes can be recorded as much as possible and the high rate is to ensure a high time resolution of encoder signal from the free end of AC motor, which is important to obtain an accurate phasor signal for TSA analysis.

Table 1 Gearbox specification

Gearbox	10kW Gearbox 1 (GB1) as speed reducer		10kW Gearbox 2 (GB2) as speed increaser	
	Stage 1 (High speed)	Stage 2 (Low speed)	Stage 1 (Low speed)	Stage 2 (High speed)
Tooth numbers	z_{r1}/z_{r2}=49/55	z_{r3}/z_{r4}=13/59	z_{i1}/z_{i2}=59/13	z_{i3}/z_{i4}=17/58
Contact ratio	ε_{a1}=1.521	ε_{a2}=1.469	ε_{a2}=1.469	ε_{a1}=1.521
Overlap ratio	ε_{b1}=1.289	ε_{b2}=1.289	ε_{b2}=1.289	ε_{b1}=1.289
Helix angle	β=27°, β=13°			
Pressure angle	α_n=20°			
Gear width	b=25 mm, b =36mm			
Module	m=1.25 mm, 2mmm			
Lubricants	EP320 with Kinematic Viscosity 320 mm^2/s @ 40°C, ASTM D445			

4.2 Test Methodology

The test rig was operating under the sinusoidal condition for 30 minutes first, then operating under five different loads at the first speed setting (50% of the full speed). After that, the test rig was operated at the same various loads but at the second (70% of the full speed). The detailed test conditions were shown in Figure 4. In each operating cycle 11 data records were acquired automatically by the host PC, each record having 30 second duration and starting at the time instant illustrated by the red square box in Figure 4. MSB and TSA analyses were applied to each dataset on another PC to obtain monitoring feature parameters at each hour and thus to construct monitoring trends for each gear pair, which will depicted in next section.

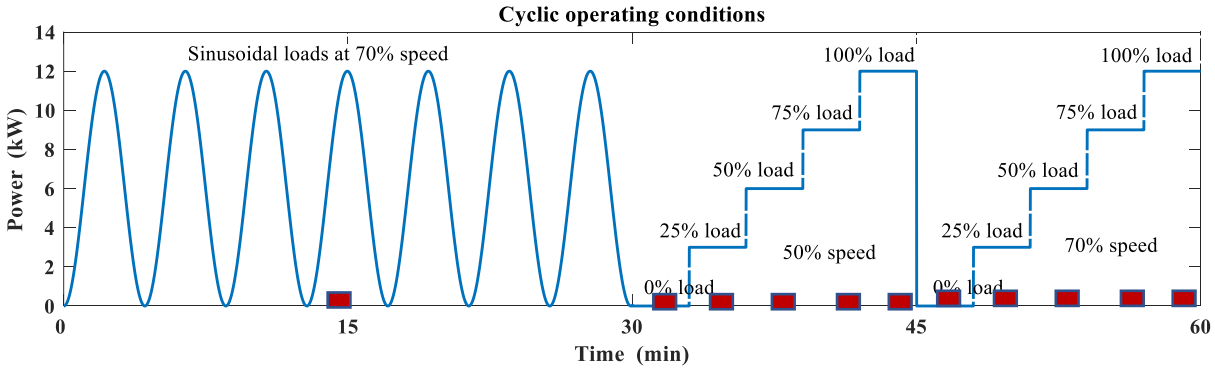

Figure 4 Load and speed profile in one operation cycle

The test was stopped after 838 hours because there were significant increases in several monitoring trends. After careful inspection when opening the gearboxes, clear wear marks and fatigue pitting were observed on the gear teeth of both gearboxes at the low speed stages. As presented in Figure 5, the visible wear marks are generated naturally on the gear tooth flanks of the low speed stages, showing that these gear conditions are severely deteriorated. On the other hand, gears at high speed stages show little changes. In addition, no clear fault signatures regarding to local faults on the bearings were seen.

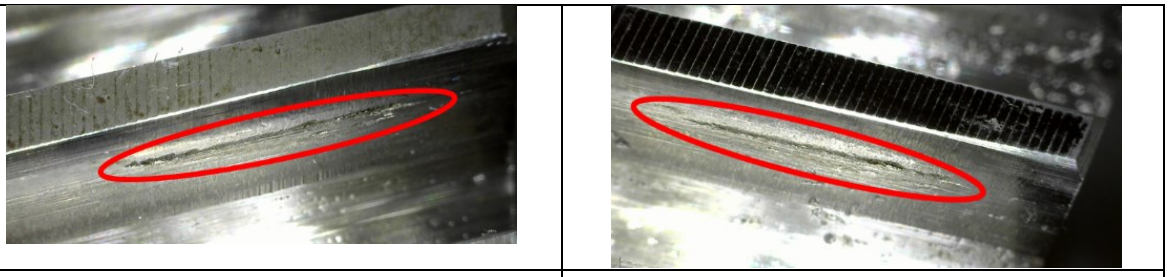

(a) wear markers on z_{r3} (b) wear markers on z_{r4}

Figure 5 Wear and pitting marks of gear teeth at low speed stages taken at 838 hours

5 MSB Analysis based Monitoring

For the online monitoring during the test operation, mesh components based monitoring parameters were calculated after applying MSB and TSA to the dataset at the higher load and speed. This section details the selection of diagnostic feature parameters and the construction of monitoring tends at early operations of the test, which then can be accurate condition indicators for achieving the diagnosis of fault locations and severity at late operating hours.

5.1 Baseline MSB Characteristics

To suppress noises in vibration signals and develop reliable diagnostic features, MSB analysis was applied to the vibration signals, which resulted in a typical MSB result shown by the 3D mesh graphs of Figure 6. For ease of discussion, the results are presented for a bifrequency range: just above $3\times f_{m2}$ and $3 \times f_{r1}$. Both MSB magnitude and coherence cover the low frequency range including several mesh frequencies and shaft frequencies of interest. They were obtained by applying Eq. (12), which reflects more on the changes in stiffness due to wear compared with Eq. (7), to the short signal segments windowed from the long signal. In total, 50 averages were achieved during MSB calculation, at which the MSB coherence becomes steady when it is averaged in the bi-frequency regions (f_r =1Hz - 60Hz, f_c =90Hz -3000Hz) that covers both the interested frequencies at both the low and high speed stages, meaning that the average is sufficiently good in suppressing the influences of random noises.

It can be seen from Figure 6 (a) that MSB magnitude shows a large number of MSB peaks on the bifrequency plane of f_c- f_r. The most significant peaks do not appear at mesh frequencies, but at f_c=250Hz, 300Hz, and 550Hz which are mainly from the AC motor as it is significantly coupled with the motor speed of f_{r1}=17.3Hz and $2f_{r1}$=34.5Hz. This coupling can be more clearly observed by MSB coherence of Figure 6 (b), in which the coherence peaks appearing at f_{r1}=17.3Hz and $2f_{r1}$=34.6Hz across nearly all f_m components. As these components are less related to gear mesh process, they need to be excluded for the focus on gear transmission monitoring.

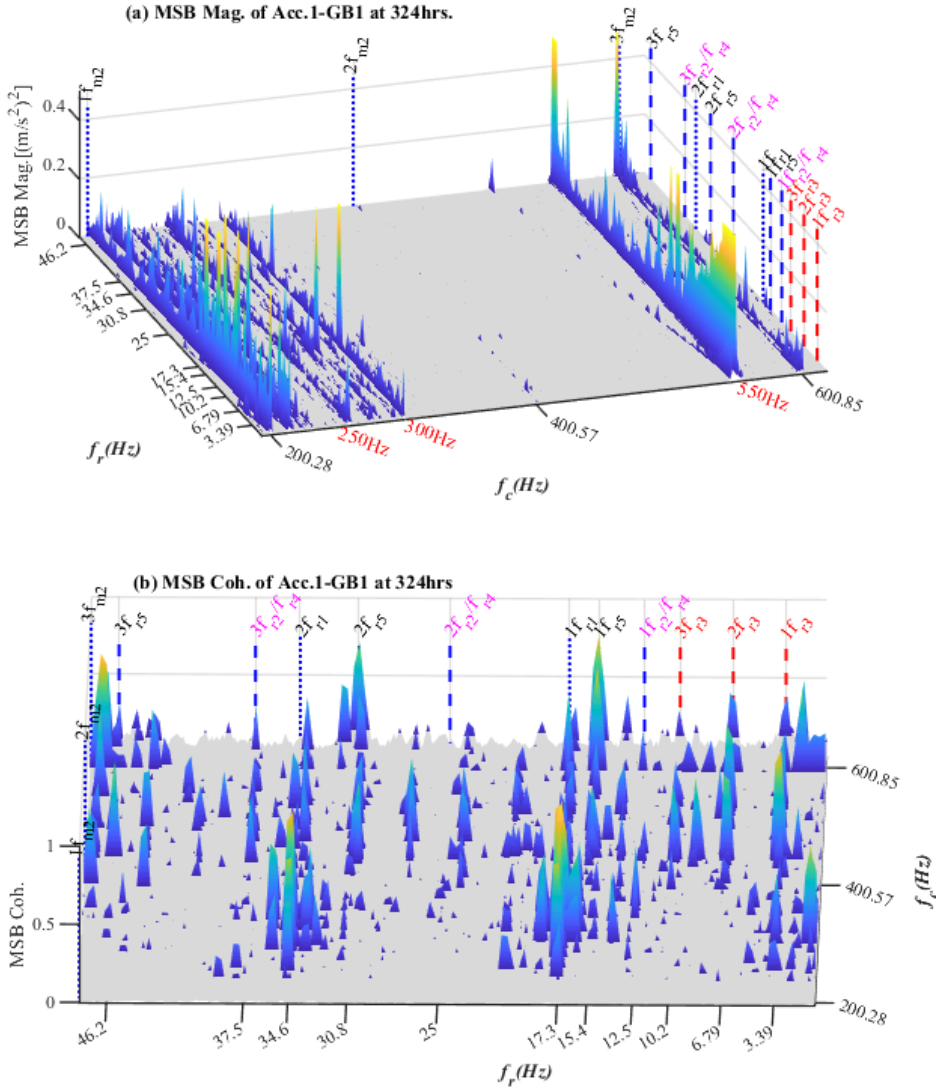

Figure 6 MSB magnitude and coherence at 324 hours

Nevertheless, MSB magnitudes show many distinctive peaks at the bifrequencies coupled between coupling gear mesh and shaft rotations that are related to gear transmission dynamics. These are more observable in the MSB coherence results of Figure 6 (b). It shows that all vibration components can be separable. Particularly, for the gear transmissions of interest, a number of MSB peaks can be observable at the low speed mesh frequencies such as f_{m2}=200.28 Hz and its three harmonics at 400.57 Hz, and 600.85 Hz. Especially, the peaks at bifrequencies of (400.57, 3.39) Hz and (400.57, 6.78) Hz indicate a clear coupling between with mesh frequency f_{m2} and the rotating frequency of shaft 3 at f_{r3} as they are all associated with the characteristic frequencies at the low-speed stage of GB1. So does for the gear rotating frequency of shaft 2 at f_{r2}. There is a peak at (400.57, 15.4) Hz. These coupling relations can be further understood by the gear arrangement shown in Figure 2. Moreover, these observable MSB peaks show that vibration signals contains sufficient information about gear dynamics and hence indicating gear health conditions. For this baseline operation, it shows that these gears have inherent imperfection including gear roundout pitch asymmetricity and eccentricity.

In addition to these peaks akin to gear dynamics, there are many other distinctive peaks shown in MSB coherence of Figure 6 (b). For example, the peak at $f_r = 1.09Hz$ which is probably due to the rotor bar asymmetricity; at $f_r = 9.29Hz$ due to the biased bearing load; and so on. These peaks can be used to assess the motor and bearing conditions respectively. These show that MSB analysis can provide

redundant information for monitoring the conditions of the whole gearbox system. Comparatively, TSA analysis cannot have these features observed simultaneously as they are not synchronous with any shaft frequencies.

To focus on monitoring gear deteriorations, 9 MSB magnitude peaks are extracted as basic monitoring and diagnostic features, which includes MSB peak magnitudes at the first 3 shaft harmonics corresponding to the first 3 meshing harmonics. In total, each gearbox results in 36 such peaks as the monitoring feature vectors. Figure 7 shows these peaks values at the baseline. It can be seen that the peaks values for the high-speed stages are generally higher than that of the low-speed stage, which is consistent with gear dynamics in that the dynamic interactions are stronger when speed is higher, and thereby confirms that vibration MSB provides reliable information for monitoring the gears. Moreover, because of the products of quadratic terms applied by MSB analysis, the values of peaks spread a wide dynamic range from 10^{-5} to 10^{+4}. This high dynamic range will be helpful to make great differences between high resolution of different conditions for diagnostics.

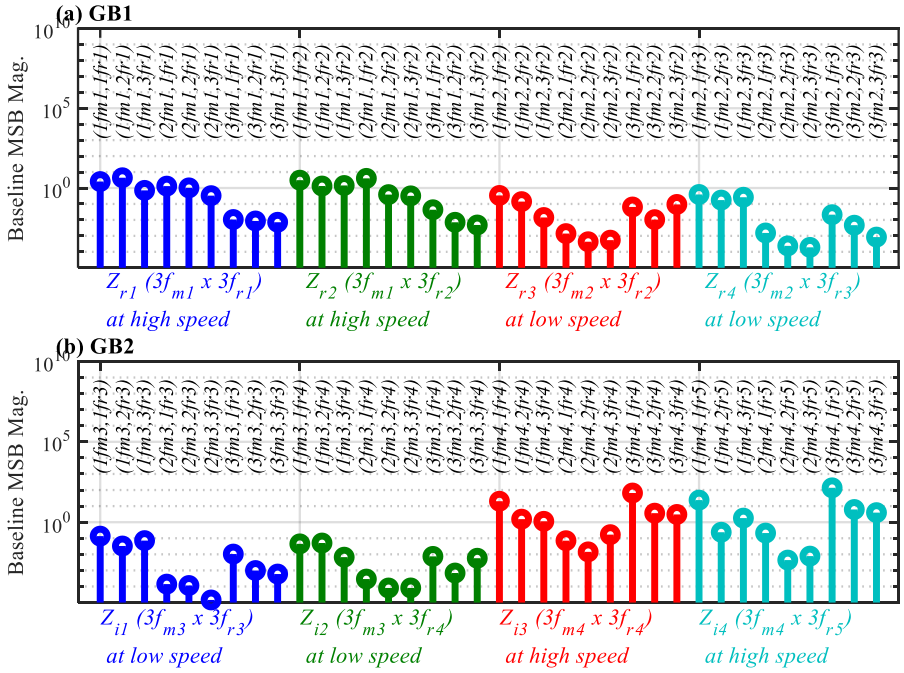

Figure 7 Baseline MSB peaks selected as diagnostic features

5.2 Gear Deterioration Indicator

Based on the characteristics of MSB amplitudes and the nonlinearity of gear dynamic effects, a gear deterioration indicator (GCI) is constructed based on MSB analysis according main following main steps:

Step 1 calculates relevant changes of MSB by normalising MSB at a time instant $|B_{MS}(nf_r, kf_c)|_{ti}$ with that of baseline time $|B_{MS}(nf_r, kf_m)|_{tb}$. By this normalisation the change in MSB at different time will be emphasised so that it reflects more the change in gear conditions at a given service time instant. It has been demonstrated by [20][21] that these relevant changes are effective to represent the changes in gear conditions when vibration and current signals are used, which is called relative MSB (rMSB) and calculated by

$$rMSB(f_r, f_m)_{ti} = \frac{|B_{MS}(nf_r, kf_m)|_{ti}}{|B_{MS}(nf_r, kf_m)|_{tb}} - 1 \tag{20}$$

Step 2 constructs a monitoring feature vector for a single gear which consists of rMSB values at the first few harmonics, in this study the harmonic order is up to 3 for both mesh and shaft rotation frequency as they allow the sufficiently reflecting changes in gear conditions and have a higher SNR as indicated by MSB coherences.

$$rMSB_{ti}(f_r, f_m)_{ti} = rMSB(1f_m, 1f_r)_{ti}\, rMSB(1f_m, 2f_r)_{ti}\, rMSB(1f_m, 3f_r)_{ti} \ldots rMSB(nf_m, kf_r)_{ti} \ldots rMSB(Nf_m, Kf_r)_{ti}\} \quad (21)$$

Step 3 calculates the mean of feature vector as one of overall MSB monitor for indicating gear conditions, which help to smooth out the variation of the changes at different harmonic numbers. The maximal value of the feature vector can be an alternative but it may have high fluctuations due to the changes are different for different harmonics. In addition, a square root is applied to the relative changes so as to highlight the contribution from smaller feature values and to further smooth out fluctuations.

$$\overline{rMSB_{ti}} = \sum_{NK} rMSB_{ti}(kf_r, nf_c)_{ti}^{1/2} \quad (22)$$

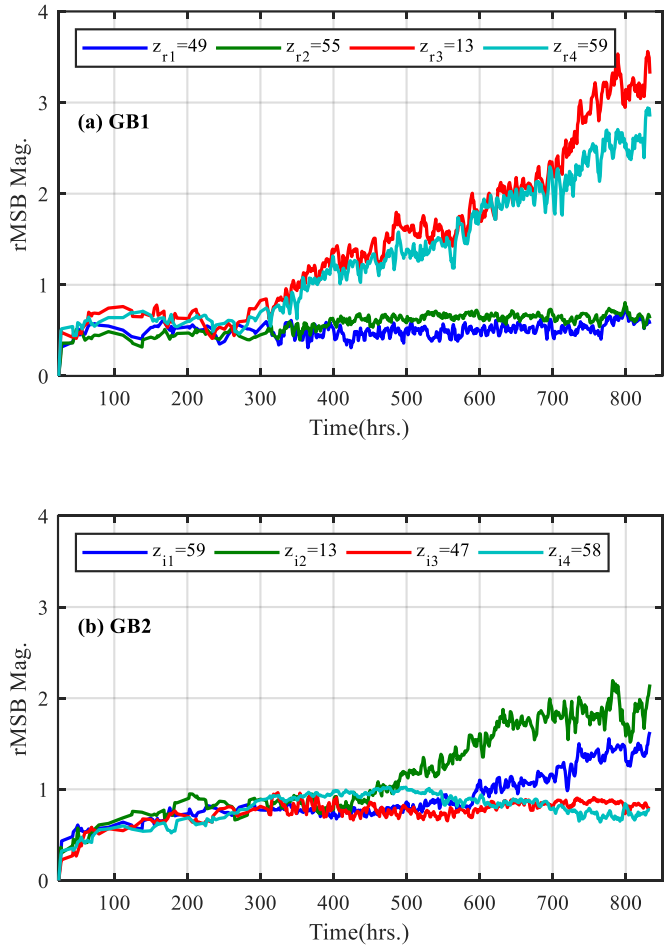

Figure 8 Relative MSB magnitudes varing with time for the 8 gears of two gearboxes

Figure 8 shows $\overline{rMSB_{ti}}$ of different gears against different operating times. It can be seen that $\overline{rMSB_{ti}}$ values exhibit different change profiles for different gears. Obviously, low speed gears show a gradual and large increase in $\overline{rMSB_{ti}}$, indicating that these gears have more deteriorations because of the significant increase in dynamic forces. In the meantime, $\overline{rMSB_{ti}}$ for the gears at high speed show slight increases. These observations agree well with the inspecting results that the tooth surfaces of low speed gears have clearer wear and pitting markers, as illustrated in Figure 5, whereas the high speed gears have little changes. This larger deterioration of low speed gears mainly attributes to lubrication influences. The low speed gears are under high load and low speed, the elastohydrodynamic (EHD)

films between tooth pairs are thinner and the surface has more wear and faster fatigue. In addition, small gears z_{r3} and z_{i2} at the low speed stages exhibit higher increase and larger amplitude compared with the large gears z_{r4} and z_{i1}. This is also very consistent with that they are subject to more load cycles and thus deteriorate more.

Interestingly, the two pairs of low speed gears show large differences in the deterioration process though they operated under the same load and speed. These differences are hard to explain but related to the manufacturing and assembly accuracy, which need to be investigated further based on the records of gear and assembly accuracy. Nevertheless, these differences including the changes in high speed gears shows further necessity of online gear condition monitoring.

In general, the relative changes of MSB magnitudes $\overline{rMSB_{tl}}$ for each gear allows a straightforward diagnosis of the location and severity of faulty gears. Especially the gradual increases can reflect the progression of the gear health conditions, which can be useful for remaining useful life prediction.

Moreover, the minimal values of GCI for GB1 is about 0.5 whereas GB2 is about 0.4 at early operations. This can be an indication that GB1 has higher dynamic forces in early operations and thus can degrade faster. Therefore, it probably explains that GB1 has deteriorated more than GB2 as it was observed by $\overline{rMSB_{tl}}$.

5.3 TSA Analysis based Monitoring

Because it is not feasible to have shaft encoder mounted at each shaft for both this test case and real applications, TSA phasor signals for different shafts or gears are calculated based on the signal pulse from the encoder at the free end of AC motor. According to gear ratios, phasors for the five shafts in Fig 3 (a) are calculated as

$$\vartheta_1 = 2\pi f_{r1} t$$

$$\vartheta_2 = 2\pi f_{r2} * t = \vartheta_1 * z_{r1}/z_{r2}$$

$$\vartheta_3 = 2\pi f_{r3} * t = \vartheta_1 * \frac{z_{r1}}{z_{r2}}\frac{z_{r3}}{z_{r4}}$$

$$\vartheta_4 = 2\pi f_{r4} * t = \vartheta_1 * \frac{z_{r1}}{z_{r2}}\frac{z_{r3}}{z_{r4}} * \frac{z_{i1}}{z_{i2}}$$

$$\vartheta_5 = 2\pi f_{r5} * t = \vartheta_1 * \frac{z_{r1}}{z_{r2}}\frac{z_{r3}}{z_{r4}} * \frac{z_{i1}}{z_{i2}}\frac{z_{i3}}{z_{i4}}$$

Based on these phasor signals, TSA signals for all gears were obtained and corresponding order spectra were calculated. Then the amplitudes at first three mesh orders and sideband orders were extracted to calculate MSB magnitudes according to Eq. (13). These coupled quadratic terms (CQT) based magnitudes allow not only for a fair comparison between the two analysis methods but also for the highlighting the interactions of dynamic forces as discussed in Sections 2 and 3. Especially, recommended feature parameters such as NA4, ER, FM4, NB4, kurtosis and so on [14] are not used in this study as they are probably not reliable for monitoring trend construction. This is because these conventional features are based on the residuals of TSA analysis which include random noises. In addition, TSA residual signals also have non-relevant signatures such as bearing faults. This can lead to an incorrect diagnosis of bearing faults.

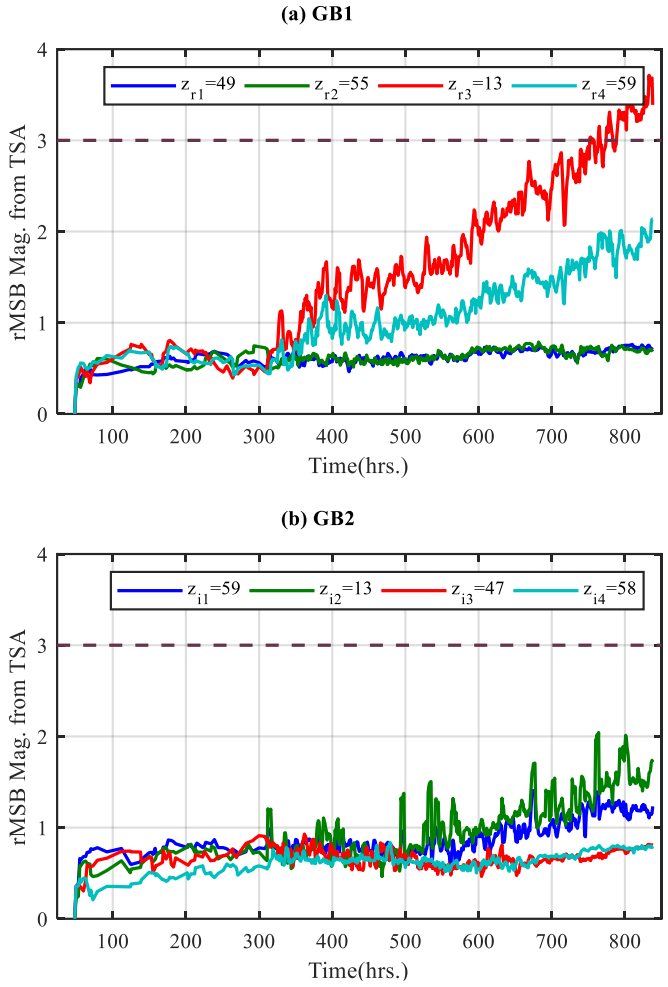

Figure 9 TSA based rMSB magnitude trends for different gears

TSA based MSB magnitude trends are shown in Figure 9. It can be seen that the results are consistent with that of MSB. It exhibits a monotonic increase trend to show the fault progression on gears z_{r3}, z_{r4}, z_{i1} and z_{i2}. However, because accumulative errors in phasor signals become higher for gears farther away from the encoder, the results are getting more deviated from that of MSB. Firstly, the amplitudes of TSA based rMSB are much smaller for gears in GB2, as shown in Figure 9 (b) and cannot indicate the significant deteriorations of gears z_{i1} and z_{i2}. This is mainly caused by the higher phase error of ϑ_4 which is accumulated over the two shafts in GB1. Secondly, the trend for the large gear z_{r4} is much lower than that of the small gear z_{r3} in GB1, as shown in Figure 9 (a). It seems reasonable as small gear z_{r3} undertakes more load cycles and has more deterioration compared with large gear z_{r4}. However, these much lower values are also caused by the phasor error as ϑ_3 is one more shaft away from ϑ_2. This error causes about 26% amplitude reduction, compared with that of MSB at the end of test runs. Overall, TSA analysis results in very low magnitudes (GB2) due to accumulative phasor errors, therefore, cannot be used to assess the health condition adequately for the entire transmission system.

6 Conclusion

Based on the presented analytic study, the time-varying stiffness of gear pair with errors including both manufacturing and those caused by deviations due to wear or pitting can be represented by modulation forms. This is because of the nonlinear interaction between the modulated responses and tooth deflections. In this way, the dynamic forces are found to be composed by the coupled quadratic terms of meshing and rotating frequency components. Furthermore, these quadratic terms are more associated

with MSB magnitudes. Therefore, MSB magnitudes can be relied on to determine the amplitudes of dynamic interactions and hence the gear condition deterioration.

Moreover, MSB analysis has a superb performance of noise suppression, which is achieved based on the internal phase invariance of modulation signals, rather than using an additional phasor signal in TSA. As a result, MSB can be implemented efficiently and conveniently to obtain an accurate trend to track the gradual gear deterioration.

Experimental validation using vibration datasets of run-to-failure tests have shown that severe deterioration of four low speed gears can be greatly indicated by more than two folds of changes in MSB magnitudes. This was in good agreement with the wear and pitting markers found by dismantling inspections. In contrast, MSB successfully detected the examined failures but TSA analysis could not do so for the deteriorations of at least two of the gears due to accumulative phasor errors

References

[1] I. Yesilyurt, F. Gu, and A. D. Ball, "Gear tooth stiffness reduction measurement using modal analysis and its use in wear fault severity assessment of spur gears," *NDT E Int.*, vol. 36, no. 5, pp. 357–372, Jul. 2003.

[2] A. Kahraman, P. Bajpai, and N. E. Anderson, "Influence of Tooth Profile Deviations on Helical Gear Wear," *J. Mech. Des.*, vol. 127, no. 4, pp. 656–663, Oct. 2004.

[3] S. Ebersbach, Z. Peng, and N. J. Kessissoglou, "The investigation of the condition and faults of a spur gearbox using vibration and wear debris analysis techniques," *Wear*, vol. 260, no. 1, pp. 16–24, Jan. 2006.

[4] G. Ibrahim, A. Albarbar, "Adaptive Filtering Based System for Extracting Gearbox Condition Feature from the Measured Vibrations", J. Measurement, 46, 2029-2034. Jul 2013.

[5] G. P. Stachowiak, G. W. Stachowiak, and P. Podsiadlo, "Automated classification of wear particles based on their surface texture and shape features," *Tribol. Int.*, vol. 41, no. 1, pp. 34–43, Jan. 2008.

[6] C. Hu, W. A. Smith, R. B. Randall, and Z. Peng, "Development of a gear vibration indicator and its application in gear wear monitoring," *Mech. Syst. Signal Process.*, vol. 76–77, pp. 319–336, Aug. 2016.

[7] Z. Peng and N. Kessissoglou, "An integrated approach to fault diagnosis of machinery using wear debris and vibration analysis," *Wear*, vol. 255, no. 7, pp. 1221–1232, Aug. 2003.

[8] J. Wojnarowski and V. Onishchenko, "Tooth wear effects on spur gear dynamics," *Mech. Mach. Theory*, vol. 38, no. 2, pp. 161–178, Feb. 2003.

[9] H. Ding and A. Kahraman, "Interactions between nonlinear spur gear dynamics and surface wear," *J. Sound Vib.*, vol. 307, no. 3, pp. 662–679, Nov. 2007.

[10] M. Lebold, K. McClintic, R. Campbell, C. Byington, and K. Maynard, "review of vibration analysis methods for gearbox diagnostics and prognostics," p. 13.

[11] G. Dalpiaz, A. Rivola, and R. Rubini, "Effectiveness and sensitivity of vibration processing techniques for local fault detection in gears," *Mech. Syst. Signal Process*, vol. 14, no. 3, pp. 387–412, May 2000.

[12] F. Combet and L. Gelman, "An automated methodology for performing time synchronous averaging of a gearbox signal without speed sensor," *Mech. Syst. Signal Process.*, vol. 21, no. 6, pp. 2590–2606, Aug. 2007.

[13] Wang, T., Han, Q., Chu, F. and Feng, Z., 2019. Vibration based condition monitoring and fault diagnosis of wind turbine planetary gearbox: A review. Mechanical Systems and Signal Processing, 126, pp.662-685.

[14] .Večeř, P., Kreidl, M. and Šmíd, R., 2005. Condition indicators for gearbox condition monitoring systems. Acta Polytechnica, 45(6).

[15] SHEN, G.J., TAO, L.M. and XU, Y.C., 2007. Research on phase error accumulation effect of time synchronous averaging. Journal of Vibration Engineering, 4.

[16] Gu, F., Shao, Y., Hu, N., Naid, A. and Ball, A.D., 2011. Electrical motor current signal analysis using a modified bispectrum for fault diagnosis of downstream mechanical equipment. Mechanical Systems and Signal Processing, 25(1), pp.360-372.
[17] F. Gu, T. Wang, A. Alwodai, X. Tian, Y. Shao, and A. D. Ball, "A new method of accurate broken rotor bar diagnosis based on modulation signal bispectrum analysis of motor current signals," *Mech. Syst. Signal Process.*, vol. 50–51, pp. 400–413, Jan. 2015.
[18] X. Tian, J. Xi Gu, I. Rehab, G. M. Abdalla, F. Gu, and A. D. Ball, "A robust detector for rolling element bearing condition monitoring based on the modulation signal bispectrum and its performance evaluation against the Kurtogram," *Mech. Syst. Signal Process.*, vol. 100, pp. 167–187, Feb. 2018.
[19] Hamomd, O., Alabied, S., Xu, Y., Daraz, A., Gu, F. and Ball, A., 2017, September. Vibration based centrifugal pump fault diagnosis based on modulation signal bispectrum analysis. In 2017 23rd International Conference on Automation and Computing (ICAC) (pp. 1-5). IEEE
[20] R. Zhang, F. Gu, H. Mansaf, T. Wang, and A. D. Ball, "Gear wear monitoring by modulation signal bispectrum based on motor current signal analysis," *Mech. Syst. Signal Process.*, vol. 94, pp. 202–213, Sep. 2017.
[21] R. Zhang, X. Gu, F. Gu, T. Wang, A. D. Ball, (2017), Gear Wear Process Monitoring using a Sideband Estimator based on Modulation Signal Bispectrum, Applied Sciences, ID: applsci-180089.
[22] Brethee, K.F., Zhen, D., Gu, F. and Ball, A.D., 2017. Helical gear wear monitoring: Modelling and experimental validation. Mechanism and Machine Theory, 117, pp.210-229.
[23] Chaari, F., Baccar, W., Abbes, M.S. and Haddar, M., 2008. Effect of spalling or tooth breakage on gearmesh stiffness and dynamic response of a one-stage spur gear transmission. European Journal of Mechanics-A/Solids, 27(4), pp.691-705.
[24] Liang, X., Zhang, H., Liu, L. and Zuo, M.J., 2016. The influence of tooth pitting on the mesh stiffness of a pair of external spur gears. Mechanism and Machine Theory, 106, pp.1-15.
[25] O. D. Mohammed, M. Rantatalo, J. Aidanpää, U.Kumar, Vibration signal analysis for gear fault diagnosis with various crack progression scenarios, Mechanical Systems and Signal Processing 41 (2013): 176-195.
[26] McFadden, P. D., and J. D. Smith. "A signal processing technique for detecting local defects in a gear from the signal average of the vibration." Proceedings of the Institution of Mechanical Engineers, Part C: Journal of Mechanical Engineering Science 199.4 (1985): 287-292.
[27] Feng, Z. and Zuo, M.J., 2012. Vibration signal models for fault diagnosis of planetary gearboxes. Journal of Sound and Vibration, 331(22), pp.4919-4939.
[28] Ahmaida, A., Zhen, D., Gu, F. and Ball, A. (2014) 'Gear wear process monitoring using acoustic signals'. In: 21st International Congress on Sound and Vibration, 13th - 17th July, 2014, Beijing, China.
[29] Yang, X., Ding, K. and He, G., 2019. Phenomenon-model-based AM-FM vibration mechanism of faulty spur gear. Mechanical Systems and Signal Processing, 134, p.106366.
[30] V.K. Tamminana, A. Kahraman, S. Vijayakar, An investigation of the relationship between the dynamic transmission error and dynamic factors of a spur gear pair, Journal of Mechanical Design, (2005).
[31] Lei, Y., Liu, Z., Wang, D., Yang, X., Liu, H. and Lin, J., 2018. A probability distribution model of tooth pits for evaluating time-varying mesh stiffness of pitting gears. Mechanical Systems and Signal Processing, 106, pp.355-366.
[32] Kundu, P., Darpe, A.K. and Kulkarni, M.S., 2019. A correlation coefficient based vibration indicator for detecting natural pitting progression in spur gears. Mechanical Systems and Signal Processing, 129, pp.741-763.